RSC Advances

PAPER

View Article Online
View Journal | View Issue

Cite this: *RSC Adv.*, 2016, **6**, 108840

Rapid, *in situ* plasma functionalization of carbon nanotubes for improved CNT/epoxy composites†

Rachit Malik,[a] Colin McConnell,[b] Noe T. Alvarez,[b] Mark Haase,[b] Seyram Gbordzoe[a] and Vesselin Shanov*[ab]

Received 16th September 2016
Accepted 10th November 2016

DOI: 10.1039/c6ra23103a

www.rsc.org/advances

Improved CNT/epoxy composites composed of dry-drawn, aligned and functionalized CNTs were fabricated. Dry-drawn multi-walled carbon nanotube (MWNTs) were functionalized by atmospheric pressure He/O_2 based plasma during the manufacturing of the CNT sheets and epoxy resin dissolved in solvent was sprayed during the manufacturing. The extent of CNT functionalization was controlled by adjusting the plasma power and flow rate of oxygen. Functionalized CNTs were characterized by Raman, X-ray Photoelectron Spectroscopy (XPS) and contact angle testing. The % wt CNT content in the composites was controlled by adjusting the concentration of epoxy in the solution used for spraying. CNTs functionalized by 100 W plasma and 63% wt CNT content produced the best composites demonstrating 43% improvement in tensile strength and 78% improvement in modulus over composites made with pristine CNTs. High % wt CNT content in the composites allow for the creation of strong, light-weight composites demonstrating specific strength as high as 918 MPa g^{-1} cm^{-3}, a 55% and 50% improvement over pristine CNT sheet and CNT/epoxy composite made with pristine CNTs, respectively.

1. Introduction

Carbon nanotubes have garnered immense interest from researchers because of their unique structure and properties. At the nanoscale, they exhibit very high strength, electrical and thermal conductivities.[1–4] These properties make CNTs an ideal reinforcement for the development of high-strength polymer/carbon nanotube composites.[5,6] Since the first report on the development of CNT/polymer composites in 1994, there have been a plethora of publications presenting various techniques for manufacturing, processing and highlighting the improvement in properties of polymer/CNT composites over that of neat polymers. Powdered CNTs involving dispersion have been extensively used but pose problems related to entanglement and aggregation.[7,8] This restricts the percent weight (% wt) of CNT content in the composite which in turn puts limits on the improvement in mechanical properties of the composite. Despite studies reporting on improvements in dispersion *via* covalent[9,10] and non-covalent functionalization[11,12] of carbon nanotubes, the random orientation of the CNTs in the 'buckypapers' and their composites confines the realization of the full potential of CNTs.

There have also been significant advancements made in the synthesis of multi-walled carbon nanotubes *via* chemical vapor deposition (CVD).[13] The discovery of 'spinnability' in CNT arrays[14] as well as the development of the floating catalyst chemical vapor deposition (FCCVD) process[15] have enabled the relatively easy manufacture of macroscale CNT assemblages such as sheets[16] and threads.[17] These assemblages have also been incorporated within polymer matrices to produce CNT/polymer composites with improved properties.[18–20] However, the mechanical properties of these assemblages and their composites are still limited by the strength of the physical van der Waals forces between CNTs and the polymer matrix. The fracture cross-section analysis reveals that the failure occurs primarily due to weak inter-tube interactions which facilitate sliding of CNTs past one another.[21,22] Therefore, it is vital to improve the interaction between nanotubes possibly by formation of covalent bonds between the CNTs themselves as well as between the CNTs and surrounding polymer matrix.

Theoretical and experimental studies on 'crosslinking' of carbon nanotubes have revealed that the load transfer between nanotubes can be enhanced by creating optimum number of defects/crosslinks.[23,24] Typically, the first step towards introducing defect sites/functional groups on CNT sidewalls has been wet chemical treatments with acids and oxidizing agents.[25] These techniques allow the creation of oxygen based functional groups such as hydroxyl (–OH), carbonyl (–C=O) and carboxyl groups on the CNTs. Functionalized CNTs and their composites have demonstrated improved properties over their non-functionalized/pristine CNT counterparts.[26,27] However, due to the inherent chemical stability of the CNT structure, these processes require treatment times ranging from minutes to

[a]*Department of Mechanical & Materials Engineering, University of Cincinnati, Cincinnati, OH, USA. E-mail: shanovvn@ucmail.uc.edu*

[b]*Department of Biomedical, Chemical and Environmental Engineering, University of Cincinnati, Cincinnati, OH, USA*

† Electronic supplementary information (ESI) available. See DOI: 10.1039/c6ra23103a

hours. The long treatment time along with the wet processing nature has limited their commercial application for functionalization of macro-scale CNT assemblages. Crosslinking by treatment with high-energy radiation such as e-beam[28] and gamma rays[29] has also shown promise towards the development of high-strength CNT materials. However, the exorbitant cost involved in scale-up of these techniques has prevented their commercial application for treatment of CNTs.

Plasma treatment as a fast, clean and dry functionalization technique has been gaining popularity as plasma technology has evolved from low pressure, chamber methods[30] to atmospheric pressure dielectric barrier discharge.[31,32] Several studies utilizing powdered CNTs have shown the potential of plasma treatment as a fast and efficient method to create a range of functional groups by varying the active gas and parameters such as power and treatment time.[33–36] Plasma functionalized CNTs incorporated within polymers such as epoxy have been shown to improve the properties of the composites over those made with pristine CNTs.[37,38] Ozone and oxygen plasma[39] have been used to efficiently functionalize CNT assemblages while still maintaining their structural stability. However, literature on the application of plasma functionalization for dry-spun CNTs and their incorporation with polymers is scarce.[40] Herein, we present an innovative approach to rapidly functionalize dry-spun CNTs from 'spinnable' arrays with oxygen-based functional groups using atmospheric pressure plasma. The plasma treatment has been integrated into a "layer-by-layer" manufacturing process of CNT/epoxy composites, which to the best of our knowledge has not been reported before. Fast, clean hydroxyl functionalization by He/O_2 plasma enables the development of composites which demonstrate over 93% improvement in tensile strength compared to pure, untreated CNT sheets.

2. Experimental section

2.1. Materials

Multi-walled carbon nanotube (MWCNT) arrays used in this study were synthesized in the form of vertically aligned, 'spinnable' carpet and the synthesis method was reported elsewhere.[13,41] The epoxy resin used in this study is API-60 obtained from Applied Poleramic Inc. It is a one-part amine-cured, toughened epoxy resin. It is supplied as a solid mixture of 4,4′-methylenebis(*N*,*N*-diglycidylaniline) (20–70%) and *N*,*N*-diglycidyl-4-glycidyloxyaniline (1–20%), tetra-functional and tri-functional epoxy resins respectively with proprietary aromatic amine curing agents (5–50%) and thermoplastic toughener (1–10%).[42] This resin is supplied is supplied as a highly viscous solid and is analogous to Hexcel Hexply™ 8552, a one-part prepreg epoxy resin which is typically supplied with unidirectional or woven carbon or glass fibers. Fig. S1 (ESI†) shows the chemical structure of the epoxy molecules present in the resin obtained from the MSDS provided by the manufacturer. The identity of the amine curing agents is not disclosed by the manufacturer in the MSDS for proprietary reasons. However, a patent filed by the manufacturer may provide some insight in to the chemical structure of the curing agents used.[43] One-part epoxy resin used in this study (API-60) was obtained from Applied Poleramic Inc. Toluene (HPLC) and dimethylformamide (DMF) (anhydrous, amine free, 99.9%) were purchased from Fisher Scientific and Alfa Aesar respectively.

2.2. Layer-by-layer manufacturing of CNT sheets

The fabrication of CNT sheets from vertically aligned CNT arrays has been reported previously.[16,44] Briefly, it involves dry-drawing of a continuous ribbon of CNTs held together by van der Waals forces. The tubes are mechanically interlocked and aligned in the direction of pulling. The end of the ribbon was then attached to a rotating cylinder covered with a Teflon™ foil. In our experiments, the speed of the cylinder rotation was so adjusted that the ribbon was drawn from the array at a rate of 1 cm s^{-1}. CNT sheets were manufactured by drawing and winding thus accumulating 10 layers of the ribbon on the cylinder at a time. After this the ribbon was detached from the rotating cylinder and the 10-layer CNT sheet was sprayed with a solvent mixture of 66 : 34 toluene : DMF, respectively. The gradual evaporation of the solvent enables the 'densification' of the CNT ribbons into a compact CNT sheet. After drying the 10-layer sheet the process was repeated 10 times to prepare a final CNT sheet comprised of 100 layers. All sheets manufactured as part of this study are comprised of 100 layers of CNT ribbon.

2.3. *In situ* plasma functionalization

The plasma functionalization was carried out with an Atomflo™ 400D plasma system from Surfx Technologies LLC. Plasma flux was generated downstream from a 25 mm diameter cylindrical torch powered by an RF generator operating at 13.56 MHz. Helium (99.999%) flowing at 15 L min^{-1} was used to generate and sustain the plasma and oxygen (99.999%) was added as the active gas for functionalization. Fig. 1(a) illustrates a schematic of the process shows the manufacturing process. Functionalized CNT sheets are manufactured by positioning the plasma torch between the CNT array and the rotating cylinder at a distance of 4.0 mm above the ribbon. The ribbon was functionalized at a rate of 1 cm s^{-1} as it passed under the plasma torch (Fig. 1(b)). The effective extent of functionalization was varied by changing the plasma power in conjunction with the oxygen flow-rate as per Table 1.

2.4. Manufacturing of CNT/epoxy composites

CNT/epoxy sheet composites were manufactured by following the "10-layer-at-a-time" process described above and adding varying amount of epoxy resin to the toluene : DMF solvent mixture. After accumulation of 100 layers of CNT ribbon, the resulting sheet was removed from the cylinder by detaching from the underlying Teflon™ film. The manufacturing process was completed by curing the CNT/epoxy sheet composites in a vacuum bag under 10 MPa pressure applied in a tetrahedron MTP-14 hydraulic hot press. The curing was carried out by heating at 107.22 °C (225 °F) for 1 hour followed by heating at 176.66 °C (350 °F) for 2 hours followed by cool down to room temperature as suggested by the manufacturer. Pristine CNT

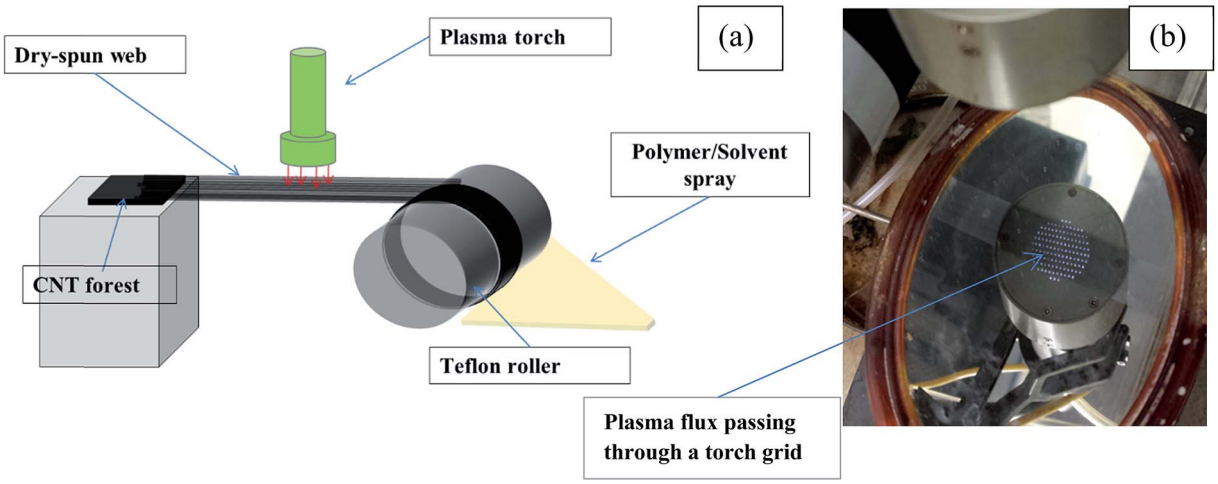

Fig. 1 (a) Schematic of the manufacturing plasma functionalized CNT sheets and composites. (b) Image of single layer of CNT ribbon passing under He/O_2 plasma torch before getting wound on the cylinder. The mirror image illustrates the plasma flux passing through a torch grid.

sheets without epoxy resin were processed under similar conditions and used as control samples.

2.5. Characterization

The extent of functionalization of CNTs was ascertained qualitatively by Raman spectroscopy (Renishaw inVia Raman Microscope, Ar-ion laser with excitation wavelength of 514 nm). Semi-quantitative analysis of % oxygen and type of functionalization was determined *via* X-ray photoelectron spectroscopy (ESCALAB PHI-5300, Mg K-alpha X-rays accelerated at 15 kV). Thermogravimetric analysis (Netzsch STA-409PC TA-DSC) was carried out by heating the samples in nitrogen (99.999%) flow of 100 mL min^{-1} at a rate of 5 °C min^{-1} up to 800 °C. The CNT sheet composites were cut using a laser micromachining system (Oxford Lasers, 532 nm solid state laser, 4 W, 5 kHz). Specimen width (~950 μm) and thickness were measured using an optical microscope (Keyence VHX-2000) and Scanning Electron Microscope (SEM, FEI XL30). Mechanical testing was carried out using an Instron 5948 Microtester equipped with a 100 N load cell. The composites prepared in this study were manufactured with the intention of achieving a high CNT mass fraction. The high % wt CNT content lends high modulus of elasticity to the composite. Due to the high modulus and very low thicknesses of our samples (~4–6 μm) we opted to test the samples at a strain rate of 1 mm min^{-1}. These specifications are in accordance with ASTM D3039 – "Standard Test Method for Tensile Properties of Polymer Matrix Composite".[45] Testing at a strain rate of 1 mm min^{-1} resulted in fracture of the specimen in 0.5–5 minutes. On the other hand, ASTM D638 – "Standard Test Method for Tensile Properties of Plastics"[46] is recommended for plastic materials or for composites with very high polymer content. ASTM D638 generally recommends a strain rate 5–500 mm min^{-1}. Such high strain rates are more suited for testing plastic specimens which typically have lower modulus and larger strain to failure as compared to CNT sheets and high wt% CNT/polymer composites. Samples for tensile testing were prepared by mounting the specimens on paper tabs with super glue and double-sided adhesive tape to prevent slipping. Ten specimens 60 mm long and 1 mm wide were used to prepare test specimens with 40 mm gauge length and were tested at a constant strain rate of 1 mm min^{-1}. A length of 10 mm on each side of the specimen was kept for retaining a good grip throughout the test. The long gauge length was used to promote fracture of the sample in the gauge section. These sample specifications are similar to those reported previously[47–53] for CNT/polymer sheet composites with high % wt CNT content. The structure, morphology and cross-section imaging of the CNT sheet composites were obtained by SEM. The volumetric density of the specimens was calculated by using the weight of specimens measured with a microbalance (Sartorius ME5) with a weight resolution of 1 μg.

Table 1 Varied plasma power (W) employed for functionalization in accordance with changing oxygen flow rate (L min^{-1})

Plasma power (W)	Helium flow rate (L min^{-1})	Oxygen flow rate (L min^{-1})
0 W	15.0	—
80 W	15.0	0.05
100 W	15.0	0.1
120 W	15.0	0.15
140 W	15.0	0.2

3. Results & discussion

3.1. Chemical & structural characterization of plasma functionalized CNT sheets

Raman spectrum obtained from multiwalled CNTs typically shows 3 peaks *viz.* D-band (~1350 cm^{-1}), G-band (~1585 cm^{-1}) and G′-band (~2700 cm^{-1}). The G band represents the graphitic nature of CNTs indicative of sp^2 hybridized carbon atoms connected *via* conjugated double bonds. The D-band on the other hand signifies the presence of sp^3 or single bonded carbon

atoms which can also provide an indication of defects and broken sp^2 bonds in the sidewalls of MWNTs. The D-band also signals the presence of carbonaceous impurities with sp^3 bonding. The G′ band symbolizes long-range order in the sample and is a result of two-phonon, second order scattering process. Plasma functionalization of CNTs results in creation of defects on the sidewalls. The creation of new defect sites causes an increase in the relative intensity of D-band from 0.57 for untreated/pristine CNTs (0 W) to 0.79 for CNTs treated with 100 W plasma (100 W), as shown in Fig. 2(a). The spectra are presented with peaks normalized by the intensity of the G-band presented as 1.0. I_D/I_G ratios were obtained for other samples treated under different plasma conditions as shown in Fig. 2(b). Relative ratios of the peak intensities as opposed to absolute peak intensities are reported since the ratios are less sensitive to instrument and atmospheric conditions, which can cause huge variations in absolute intensities. As expected, there is a gradual increase in the I_D/I_G ratio with increase in the plasma power and the resulting increase in concentration of reactive oxygen species in the plasma zone. The use of oxygen as active gas in plasma functionalization of CNTs has been shown to create defect sites with oxygen based functional groups.[32]

The presence of these functional groups is confirmed *via* surface analysis of CNT sheets by X-ray Photoelectron Spectroscopy (XPS). Fig. 3(a) shows the XPS survey scans indicating carbon and oxygen core peaks at ~284.6 eV and ~532 eV respectively. 100 W plasma treated CNT sheet shows an increase

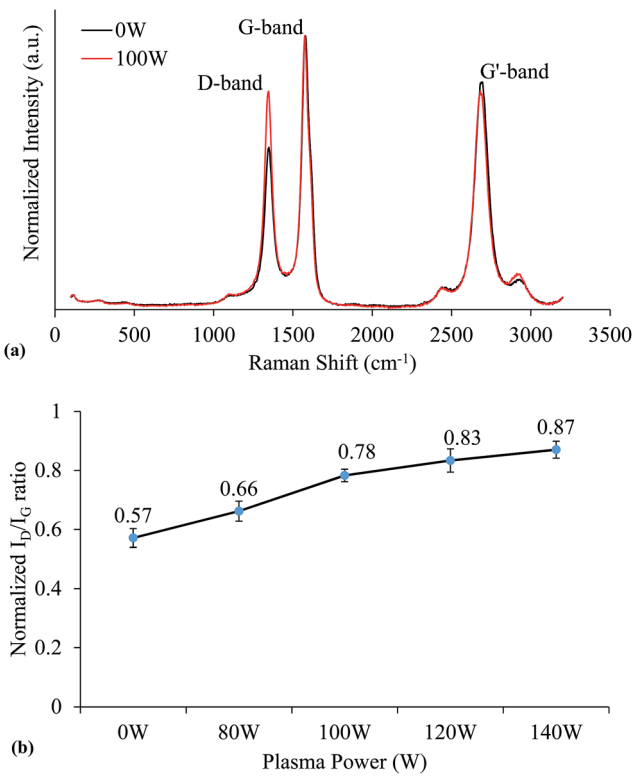

Fig. 2 (a) Raman spectra showing comparison between pristine (0 W) and 100 W plasma treated CNT sheets; (b) variation of normalized I_D/I_G Raman ratios for CNT sheets processed with varying plasma power.

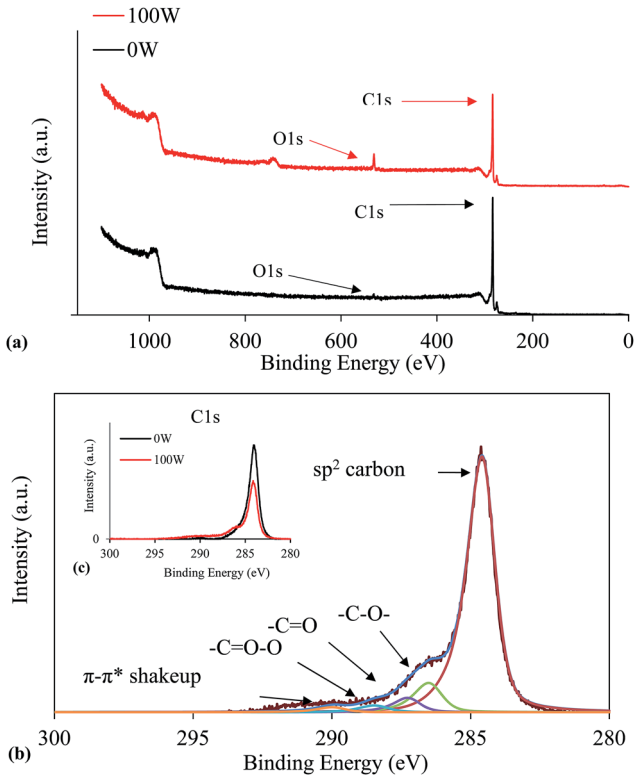

Fig. 3 (a) XPS survey scans of pristine (0 W) and plasma treated (100 W) CNT sheets; (b) high-resolution C1s scan of 100 W plasma treated sheets highlighting the different oxygen-based functional groups; (c) inset plot comparing C1s spectral features between 0 W (untreated) and 100 W plasma treated CNT sheets.

to 6.7% of O-content in contrast to 1.1% for pristine (0 W) CNT sheet. Fig. 3(b) shows a de-convoluted high-resolution multiplex C1s scan of 100 W plasma treated CNT sheet wherein integrated (Shirley) background was subtracted, and every curve fit component peak utilized the same asymmetric GL(30) (Gaussian/Lorentzian product) peak shape and FWHM (Full Width at Half Maximum). The de-convoluted spectrum comprises of five peaks which are curve-fitted with the most prominent peak centered at 284.6 eV representing C=C sp^2 hybridized graphitic carbon. The peaks centered at 286.4, 287.2 and 288.6 eV represent the bonds formed between carbon and oxygen leading to the creation of hydroxyl (–OH), carbonyl (–C=O–) and carboxyl (–C=O–O–) groups respectively. The peak centered at 290.0 eV represents π–π* shakeup satellite (290.67 eV), and is not indicative for a functional group, but can be considered as evidence of conjugation existing within the nanotube's structure. The results from deconvolution and curve-fitting of XPS data are consistent with previously reported results in literature.[54]

The % O content on the CNT sheet surface increases with a rise in plasma power as shown in Fig. 4(a). Most oxygen atoms attached to CNTs are bonded in the form of hydroxyl and carbonyl groups. Table 2 presents a summary of the XPS results showing % contribution of different functional groups from curve-fitting C1s spectra of plasma functionalized CNT sheets. The creation of hydroxyl groups enhances the probability of

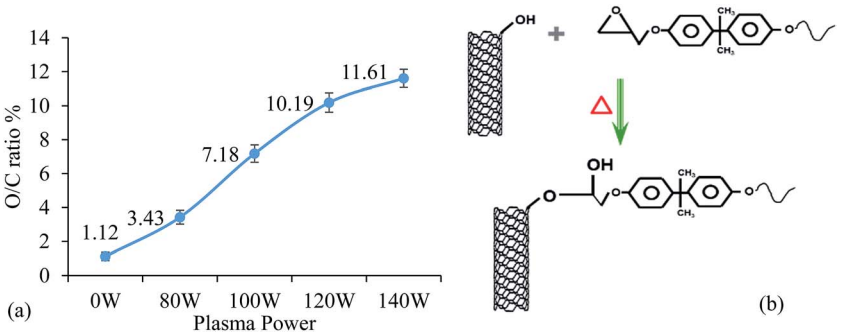

Fig. 4 (a) O/C ratio obtained from XPS analysis of CNT sheets functionalized by plasma; (b) reaction between –OH functionalized CNT and epoxide functional resin.

covalent bonding between CNTs and epoxy resin as illustrated in the reaction scheme shown in Fig. 4(b).

Plasma functionalization and creation of hydroxyl groups allows CNTs to interact with water thereby altering their hydrophobic nature. Contact angle testing on CNT sheets visualized by a drop of deionized (D.I.) water was measured using Model 590 Rame-hart Contact Angle Goniometer. Fig. 5 shows images of the droplet of water on pristine and plasma treated sheets (100 W & 120 W). The measured contact angle for the CNT sheet drops from an average of 79.6° for the pristine sheet to 14.2° for the plasma treated samples, showing the increased affinity to water of the plasma treated sheet. These results have been observed and reported previously[32,39,55] and can explained on the premise that water can associate with the plasma functionalized CNT sheet *via* hydrogen bonding with the oxygen-based functional groups on the CNT surface.

3.2. Mechanical properties of CNT/epoxy composite sheets

The merits of spraying liquid polymer in between the layers of the CNT ribbon has been reported previously by Liu *et al.*[56] In their experiments, they sprayed polyvinyl alcohol (PVA) dissolved in ethanol/water mixture. We initially attempted to spray the polymer solution while winding the CNT ribbon but due to the high boiling points of the solvents we used, it allowed the ribbon on the cylinder to stay wet. The wet ribbon results in a loss of friction at the point where the new ribbon is accumulated on the cylinder causing the ribbon to eventually break off the rotating cylinder. Liu *et al.*[56] did not report any such issue in their process which could be attributed to: (a) the relatively lower boiling point of their solvent system, and (b) the small width of their CNT ribbon (3–5 mm) *vs.* our ribbon (10–15 mm). Small ribbon width would minimize chances of failure.

Table 2 Summary of XPS curve-fit data from pristine and plasma functionalized CNT sheets

Sample type	C=C sp^2 (%)	C–OH (%)	C=O (%)	C=O–O–H (%)	π–π^* shakeup (%)
0 W	94.8	1.9	1.3	0.3	1.7
80 W	85	7.2	5.7	1.0	1.1
100 W	82.6	8.3	6.8	1.3	1.0
120 W	80.5	9.5	6.5	2.7	0.8
140 W	79.1	9.9	7.0	3.2	0.8

CNT/epoxy composites were manufactured by using different concentrations of epoxy solutions *viz.* 0.1, 0.25, 0.5 & 1.0% wt/vol in 66 : 34 toluene : DMF solvent mixture. The composites were characterized by thermo-gravimetric analysis (TGA) by heating in N_2 atmosphere to 900 °C at 5 °C min^{-1}. Fig. 6(a) shows the thermogravimetric profiles of the CNT/epoxy composites compared to that of pure epoxy. Pure, cured epoxy resin undergoes peak degradation at 385 °C and leaves behind ~30% residual mass/char. CNT sheet undergoes negligible change in mass (~1.01%) during the same thermal treatment. Therefore, if the mass loss exhibited by CNT/epoxy composites is primarily the mass lost by the epoxy component of the composite, one can calculate % wt CNT in the composites using the following equation.

$$\%\ \text{wt CNT in composite} = 100 - \left(\left(\frac{\%\ \text{mass loss of composite}}{\%\ \text{mass loss of pure epoxy}}\right) \times 100\right)$$

Fig. 6(b) shows the differential thermogravimetric (DTG) plots for CNT/epoxy composites, CNT sheet and cured epoxy resin. Interestingly, epoxy composites containing CNTs show a lower peak degradation temperature, possibly indicating poorer thermal stability compared to pristine epoxy only. However, this behavior has been observed before for polymer composites containing CNTs and is attributed to the increased thermal diffusivity exhibited by the composite on addition of CNTs.[57,58] The increase in thermal diffusivity lowers the activation energy and thus the peak degradation temperature for the degradation reaction of the polymer resin.[59] The degradation temperature is also dependent on the % wt CNT content in the composite with composites containing higher % wt content exhibiting lower peak degradation temperatures as shown in Fig. 6(b). This is attributed to the high thermal diffusivities of composites with higher % wt CNT content. The presence of functional groups on CNTs can also alter their interactions with the polymer matrix and thus affect the thermal stability of the resulting composite.[58] The study of thermal properties of functionalized CNT/epoxy composites are beyond the scope of this report and shall be presented in future publications.

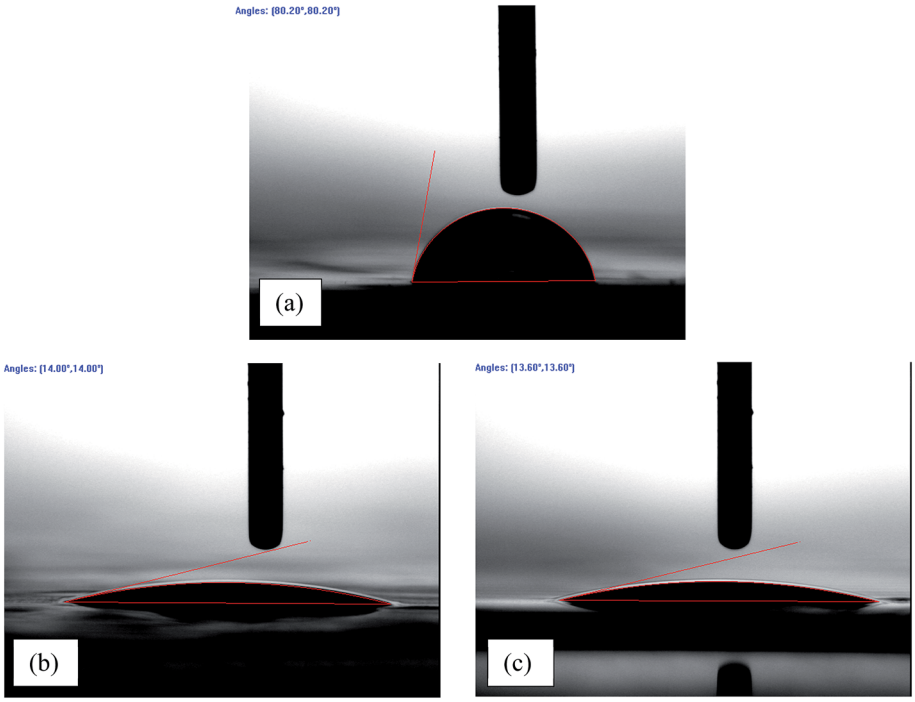

Fig. 5 Contact angle of D.I. water on (a) pristine; (b) 100 W plasma treated CNT sheet; (c) 120 W plasma treated CNT sheet.

Fig. 6(c) shows mechanical properties of CNT/epoxy composites comprised of pristine (0 W) CNTs as a function of % wt CNT content. The increase in concentration of epoxy in solution results in overall reduction of the weight% CNT content in the final composite. Composites with ~63% wt CNT content demonstrate the highest tensile strength. It should be noted however, that tensile strength is a calculated quantity dependent on the load (N) and the specimen cross-sectional area (μm × μm). The load to failure values measured for composites with ~42% wt CNT content are higher compared to that of 63% wt CNT content. This could be attributed to the increase in the amount of epoxy in the composite leading to an increased load value, but also resulting in an increase in the thickness of the sheet composite (Fig. 7(a) and (b)). Thus, the tensile strength value for composites with greater % wt epoxy is lower than those with greater % wt CNT content. Table 3 shows the variation in thickness of CNT/epoxy composites produced by varying the concentration of epoxy solution resulting in different % wt CNT content. Interestingly, composites with higher % wt CNT content (~82%) and pure CNT (100%) sheet show lower tensile strength despite having lower thickness values. The lower tensile strength in this case is a result of lower load to failure values. This is caused by the sliding of CNTs past one another in CNT sheets comprised of pristine nanotubes as the CNTs are held together by relatively weaker van der Waals forces.

3.3. Effect of plasma functionalization on mechanical properties of CNT/epoxy composites

CNT/epoxy composites with plasma functionalized CNTs were fabricated in a similar manner where the functionalization was carried out by passing the CNT ribbon under the plasma torch before winding on the rotating cylinder. The extent of functionalization was controlled by the adjusting the plasma power (W) level and the corresponding oxygen flow rate (L min^{-1}). Fig. 8(a) shows the effect of plasma power on the tensile strength and load values for CNT/epoxy composites with 63 wt% CNT content. Tensile stress of CNT/epoxy composites initially increases with the increase in plasma power reaching highest value for 100 W plasma functionalized CNT/epoxy composites. High degree of functionalization achieved by using plasma power greater than 100 W results in significant damage to the structure of the individual nanotubes, thereby negatively affecting the mechanical properties of the resulting composite. The extent of functionalization that can be controlled by the level of power and oxygen gas flow rate is critical towards the development of high-strength composites. The improvement in properties can be attributed to the reaction and crosslinking between –OH groups on functionalized CNTs and the epoxy resin. This results in much improved load transfer between individual CNTs, thereby improving the overall properties of the composite. The interaction between functionalized CNTs and the epoxy resin was confirmed by performing a controlled experiment involving reaction of functionalized CNT sheet with epoxy resin in solution. The functionalized CNT sheets were produced by *in situ* plasma treatment at 100 W. Tetra-functional epoxy resin (4,4′-methylenebis(*N*,*N*-diglycidylaniline)) was dissolved in toluene and 5 wt% solution was created. The functionalized CNT sheet was immersed in the epoxy/toluene solution in a sealed beaker and was heated on a hot plate to 90 °C with stirring for 4 hours. Upon completion of this procedure, the CNT sheet was removed from the epoxy/toluene

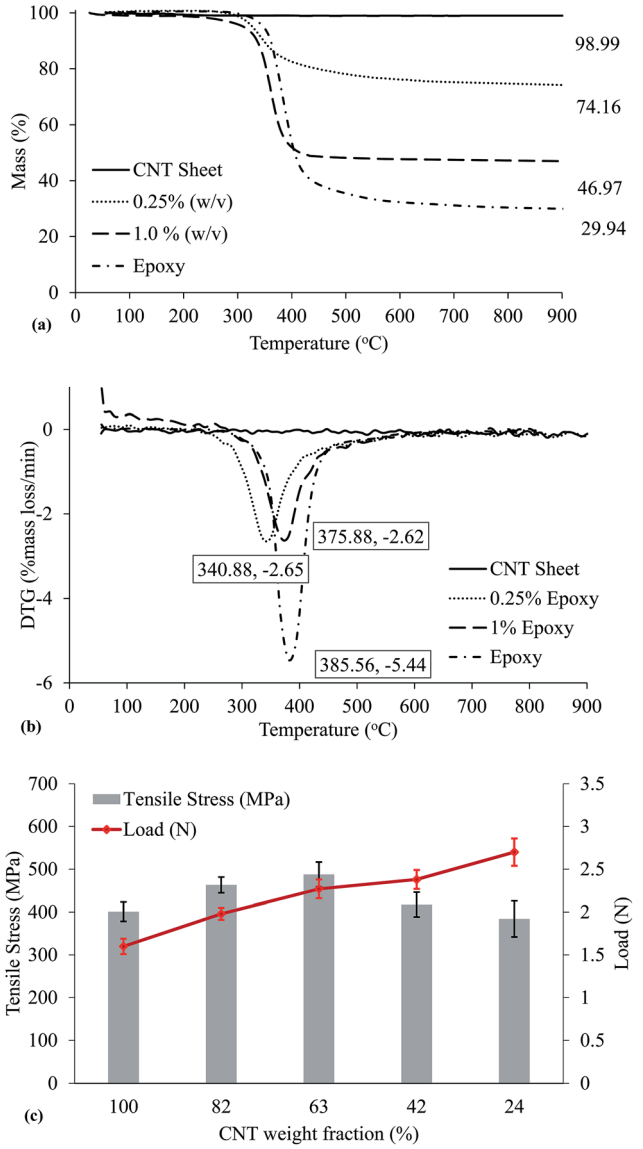

Fig. 6 (a) TGA plots of CNT sheet, pure epoxy and CNT/epoxy composites fabricated with different concentrations of epoxy in the solutions; (b) DTG profiles for CNT sheet, pure epoxy and CNT/epoxy composites fabricated with different concentrations of epoxy in the solutions; (c) mechanical properties of pristine CNT/epoxy composite as a function of % wt CNT content.

solution and washed three times with excess of hot toluene at 80 °C to remove any unreacted epoxy. After washing with toluene, the CNT sheet was dried in a vacuum oven at 80 °C for 8 hours. The dried CNT sheet was expected to react with epoxy and the resulted sample was studied by XPS. Fig. S2(a) in the ESI† shows the survey scan from the functionalized CNT sheet derivatized with epoxy which reveals 3.6% at N content. However, the survey scan of functionalized CNT sheet (Fig. S2(b)†) that was not treated with epoxy showed absence of any N peak. The epoxy resin in this derivatization experiment was used without any additional curing agent. It is important to note that the epoxy molecule contains nitrogen in the form of tertiary amines, as seen in the Fig. S1 from the ESI,† thus serving as a nitrogen precursor. Tertiary amine is known to be able to catalyze the ring opening of the epoxide group and thereby allow reaction with hydroxyl groups to take place.[60]

Crosslinking within the composite can be classified into 3 linkages *viz.* are CNT–epoxy, CNT–epoxy–CNT and epoxy–epoxy. When the composite contains functionalized CNTs and the % wt content of CNTs in the composite is high (82 & 63 wt%), CNT–epoxy and CNT–epoxy–CNT linkages can be considered dominant. Thus, the tensile strength and modulus of functionalized CNT–epoxy composites is greater than that of composites with pristine (0 W) CNTs and CNT sheet alone (Fig. 8(b)). However, when the % wt epoxy content in the final composite is increased, epoxy–epoxy linkages can be expected to dominate. This results in increased overall crosslinking which results in increase in modulus but coupled with a decrease in tensile strength as seen in data presented in Table S1.† The introduction of epoxy increases the density of the composite by filling voids between CNTs which are held together with van der Waals forces. The presence of CNTs can impede the crosslinking of epoxy molecules between (epoxy–epoxy bonding) themselves during the curing process. On increasing epoxy content, there is an increased probability of epoxy–epoxy bonding which in turn results in a relatively degree of crosslinking leading to an increase in modulus with increase in epoxy content and decrease in CNT content from 63% to 42%. However, CNTs are significantly stronger than epoxy and an increase in epoxy content causes a reduction in overall CNT content, which can lead to a relatively lower tensile stress for composites with lower CNT content (42 wt%). Here, it is important to note that the increase in modulus for 100 W plasma functionalized CNT sheets is greater than that for pristine CNT sheet when comparing composite with 63 wt% and 42 wt% CNTs. This dissimilarity can be attributed to the increased interaction between the plasma treated carbon nanotubes and the resin *via* the functional groups.

Mechanical properties of CNT sheets without epoxy show a decreasing trend after plasma functionalization with strength going down with increasing plasma power. These results are expected as the number of defects increases with increase in plasma power also shown *via* Raman spectroscopy. Similar results have been reported previously showing negative effect of plasma treatment on mechanical properties of CNT threads and buckypapers in the absence of any polymer matrix. However, on combining functionalized CNTs with epoxy and other polymers[6] numerous researchers have observed an improvement in the mechanical properties of the final composite over those made with non-functionalized/pristine CNTs. Therefore, it is essential to have control over the extent of functionalization as the optimum degree of functionalization of CNTs combined with the appropriate amount of reactive polymer resin may result in a composite with superior properties.

Plasma functionalization of buckypapers[61] and its application for improving interaction with polymer matrices has been reported previously. However, functionalization of buckypapers after manufacturing limits the penetration of the plasma flux leading to non-uniform functionalization and limited improvement in properties of resulting composites.[62] We

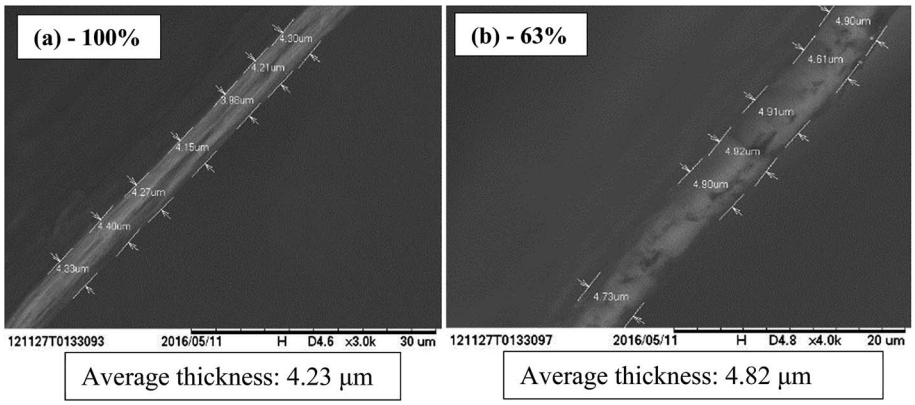

Fig. 7 (a and b) SEM images of thickness of pristine CNT sheet and CNT/epoxy composites with 63% wt CNT content, respectively.

demonstrate functionalization of CNTs during the sheet formation which allows uniform functionalization and interaction with the epoxy throughout the thickness of the composite. Majority of existing literature sources studying the interaction between functionalized CNTs and epoxy utilize powdered CNTs and the maximum % wt CNT content achieved in these reports is significantly below 50% with average ranging between 0.1 and 5%. There are multiple reports on development of CNT sheet/polymer composites comprised of aligned CNT produced by dry-spinning method.[56,63–65] However, most of these reports focused on improving techniques by mechanical methods such as stretching[66] and pressing.[67] However, none of them explored functionalization of CNTs within the sheet and its effect on the mechanical properties of CNT/polymer composites. Recently, there have been studies carried out on the effect of functionalization of CNT fibers produced by floating catalyst chemical vapor deposition (FCCVD) technique.[68] This study and others involving treatment of CNT sheets[69] and yarns[70] in a solution require disposal of the chemicals after use. Also, the treatment is carried out after the CNT assemblage has already been formed which can result in issues pertaining to penetration of functionalization solution and the resin afterwards. This results in the use of vacuum techniques to better infiltrate the polymer resin into the bulk of the CNT assemblage.[70] However, to the best of our knowledge, there are no studies reported on the functionalization of CNT sheets by atmospheric pressure plasma sheets and its effect on the mechanical properties of CNT/polymer composites. Hang *et al.*[32] used a similar plasma system to explore oxygen functionalization of CNT sheets and yarns produced by the FCCVD technique. However, their study was only focused on functionalization and they did not explore combination of functionalized CNT sheets/yarns and polymer resin to produce high strength composites. We had previously explored plasma functionalization of CNT sheets and their application in CNT/PVA composites.[71] The present study builds on the knowledge gained from our previous work and explores the effect of plasma functionalization and resin content.

Specific strength (stress normalized with density) is an important metric for evaluating structural aerospace materials. Composites with high % wt CNT content possess light-weight, which makes them good candidates for aerospace

Table 3 Variation in thickness of CNT/epoxy sheet composites produced from varying concentration of epoxy solutions

Concentration of epoxy solution (w/v, %)	Thickness of CNT/epoxy composite (μm)	% wt CNT content
0	4.23	100
0.1	4.43	82
0.25	4.82	63
0.5	5.69	42
1.0	6.54	24

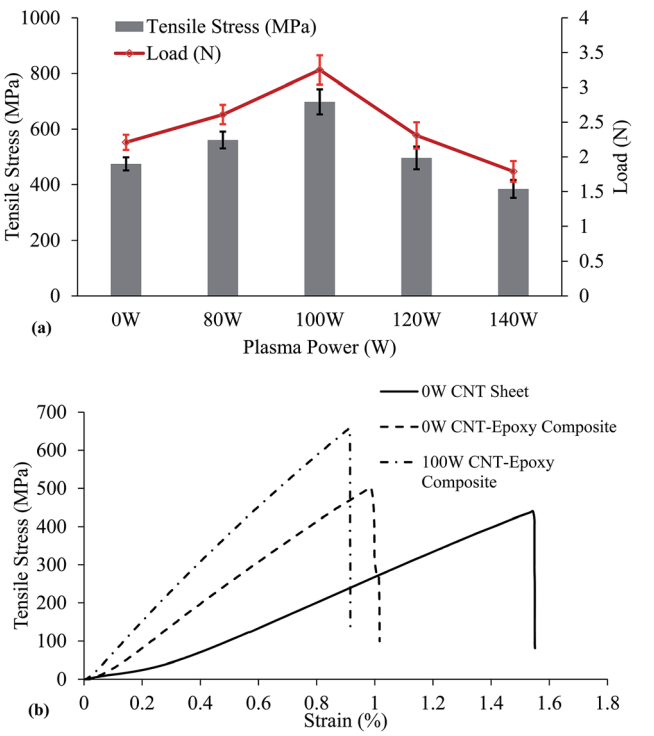

Fig. 8 (a) Mechanical properties of CNT/epoxy composite (with 63% wt CNTs) as a function of plasma power; (b) representative stress–strain curves of composites comprised of pristine and plasma functionalized CNTs compared with CNT sheet alone.

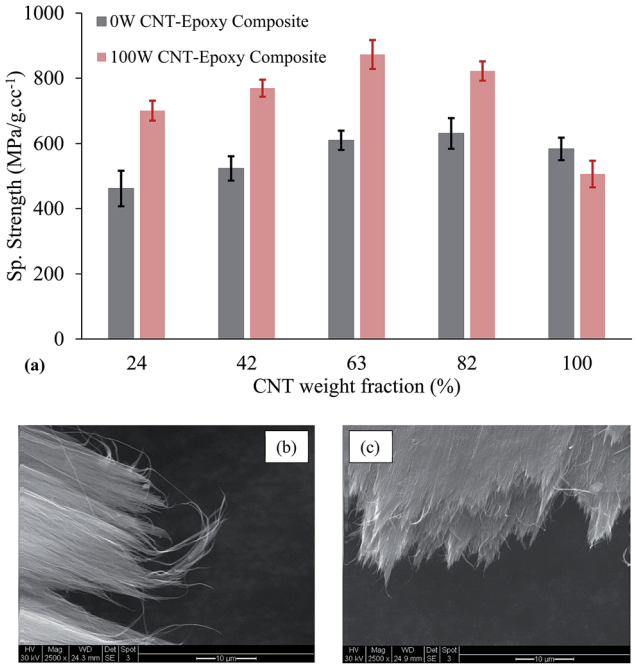

Fig. 9 (a) Specific strength of pristine and plasma functionalized CNT/epoxy composites as a function of % wt CNT content; SEM images of fractured ends of (b) pristine CNT–epoxy composite and (c) 100 W CNT–epoxy composite.

applications. The uniform functionalization and infiltration achieved in this work, while maintaining a high % wt CNT content allows us to create composites with better properties than those obtained from CNT–buckypaper/polymer composites, reported previously.[72] Fig. 9(a) shows the specific strength of CNT/epoxy composites with and without plasma functionalized CNTs. The formation of covalent crosslinks between functionalized CNTs and epoxy enables better load transfer along the length of the composite. Fig. 9(b) and (c) show the morphology of fractured ends of composites made with pristine and functionalized CNTs respectively. Pristine CNT/epoxy composites fracture unevenly with loose CNTs hanging out from the broken end possibly a result of sliding of nanotubes past each other – Fig. 9(b). The clean, relatively sharper fracture typically observed in Fig. 9(c) for functionalized CNT/epoxy composite is evidence of the formation of covalent bonds between CNTs and epoxy resin. These results demonstrate the effect of the synergy of reactive polymer resins with functionalized CNTs.

4. Conclusion

A new method of creating improved CNT based composites with *in situ* plasma functionalization has been demonstrated. Control over degree of functionalization is critical for the development of strong composites and can be easily manipulated by adjusting the plasma power and oxygen flow rate. The successful functionalization of CNTs with oxygen-based groups was confirmed and quantified by XPS. The "10-layer-at-a-time" approach allows uniform integration of the polymer matrix with CNT sheet and the % wt CNT content can be easily controlled by adjusting the amount of polymer in the solution. Atmospheric pressure plasma functionalization allows rapid, efficient and controlled functionalization of CNTs. Composites with varied extent of functionalization were manufactured and tested. CNTs functionalized with 100 W plasma combined with ~37 wt% epoxy resin demonstrated 43% improvement in tensile strength and 78% improvement in modulus over composites made with pristine CNTs. The improvement in properties obtained by addition of epoxy resin and plasma functionalization is about 70% in tensile strength and over 171% in modulus over pristine CNT sheets.

Acknowledgements

The authors would like to acknowledge the support and expertise of the team at NASA Langley Research Center. This work was funded by the National Science Foundation (NSF) through the following grants: CMMI-0727250; SNM-1120382; ERC-0812348. The authors also appreciate the support of DURIP-ONR N00014-15-1-2473; ARMY W911NF-16-2-0026 and NASA NNX13AF46A grants.

References

1 M. Yu, B. Files, S. Arepalli and R. Ruoff, *Phys. Rev. Lett.*, 2000, **84**, 5552–5555.
2 W. Ding, L. Calabri, K. M. Kohlhaas, X. Chen, D. A. Dikin and R. S. Ruoff, *Exp. Mech.*, 2007, **47**, 25–36.
3 T. W. Ebbesen, H. J. Lezec, H. Hiura, J. W. Bennett, H. F. Ghaemi and T. Thio, *Nature*, 1996, **382**, 54–56.
4 M. Yu, *Science*, 2000, **287**, 637–640.
5 Y. Liu and S. Kumar, *ACS Appl. Mater. Interfaces*, 2014, **6**, 6069–6087.
6 N. G. Sahoo, S. Rana, J. W. Cho, L. Li and S. H. Chan, *Prog. Polym. Sci.*, 2010, **35**, 837–867.
7 J. N. Coleman, M. Cadek, R. Blake, V. Nicolosi, K. P. Ryan, C. Belton, A. Fonseca, J. B. Nagy, Y. K. Gun'ko and W. J. Blau, *Adv. Funct. Mater.*, 2004, **14**, 791–798.
8 H. Deng, R. Zhang, C. T. Reynolds, E. Bilotti and T. Peijs, *Macromol. Mater. Eng.*, 2009, **294**, 749–755.
9 K. Balasubramanian and M. Burghard, *Small*, 2005, **1**, 180–192.
10 H. Park, J. Zhao and J. P. Lu, *Nano Lett.*, 2006, **6**, 916–919.
11 M. J. O'Connell, P. Boul, L. M. Ericson, C. Huffman, Y. Wang, E. Haroz, C. Kuper, J. Tour, K. D. Ausman and R. E. Smalley, *Chem. Phys. Lett.*, 2001, **342**, 265–271.
12 Y.-L. Zhao and J. F. Stoddart, *Acc. Chem. Res.*, 2009, **42**, 1161–1171.
13 V. Shanov, W. Cho, R. Malik, N. Alvarez, M. Haase, B. Ruff, N. Kienzle, T. Ochmann, D. Mast and M. Schulz, *Surf. Coat. Technol.*, 2013, **230**, 77–86.
14 K. Jiang, Q. Li and S. Fan, *Nature*, 2002, **419**, 801.
15 Y.-L. Li, I. A. Kinloch and A. H. Windle, *Science*, 2004, **304**, 276–278.

16 M. Zhang, S. Fang, A. a. Zakhidov, S. B. Lee, A. E. Aliev, C. D. Williams, K. R. Atkinson and R. H. Baughman, *Science*, 2005, **309**, 1215–1219.
17 K. Koziol, J. Vilatela, A. Moisala, M. Motta, P. Cunniff, M. Sennett and A. Windle, *Science*, 2007, **318**, 1892–1895.
18 X. Wang, P. D. Bradford, W. Liu, H. Zhao, Y. Inoue, J. P. Maria, Q. Li, F. G. Yuan and Y. Zhu, *Compos. Sci. Technol.*, 2011, **71**, 1677–1683.
19 K. Liu, Y. Sun, X. Lin, R. Zhou, J. Wang, S. Fan and K. Jiang, *ACS Nano*, 2010, **4**, 5827–5834.
20 C. D. Tran, W. Humphries, S. M. Smith, C. Huynh and S. Lucas, *Carbon*, 2009, **47**, 2662–2670.
21 X. Zhang, Q. Li, Y. Tu, Y. Li, J. Y. Coulter, L. Zheng, Y. Zhao, Q. Jia, D. E. Peterson and Y. Zhu, *Small*, 2007, **3**, 244–248.
22 J. T. Di, D. M. Hu, H. Y. Chen, Z. Z. Yong, M. H. Chen, Z. H. Feng, Y. T. Zhu and Q. W. Li, *ACS Nano*, 2012, **6**, 5457–5464.
23 M. Huhtala, A. V. Krasheninnikov, J. Aittoniemi, S. J. Stuart, K. Nordlund and K. Kaski, *Phys. Rev. B: Condens. Matter Mater. Phys.*, 2004, **70**, 45404.
24 C. F. Cornwell and C. R. Welch, *J. Chem. Phys.*, 2011, **134**, 204708.
25 V. Datsyuk, M. Kalyva, K. Papagelis, J. Parthenios, D. Tasis, A. Siokou, I. Kallitsis and C. Galiotis, *Carbon*, 2008, **46**, 833–840.
26 Z. Chen, X. J. Dai, K. Magniez, P. R. Lamb, D. Rubin de Celis Leal, B. L. Fox and X. Wang, *Composites, Part A*, 2013, **45**, 145–152.
27 Q. Cheng, B. Wang, C. Zhang and Z. Liang, *Small*, 2010, **6**, 763–767.
28 S. G. Miller, T. S. Williams, J. S. Baker, F. Solá, M. Lebron-Colon, L. S. McCorkle, N. G. Wilmoth, J. Gaier, M. Chen and M. a. Meador, *ACS Appl. Mater. Interfaces*, 2014, **6**, 6120–6126.
29 M. Miao, S. C. Hawkins, J. Y. Cai, T. R. Gengenbach, R. Knott and C. P. Huynh, *Carbon*, 2011, **49**, 4940–4947.
30 A. Felten, C. Bittencourt, J. J. Pireaux, G. Van Lier and J. C. Charlier, *J. Appl. Phys.*, 2005, **98**, 74308.
31 M. V. Naseh, A. A. Khodadadi, Y. Mortazavi, F. Pourfayaz, O. Alizadeh and M. Maghrebi, *Carbon*, 2010, **48**, 1369–1379.
32 H. Yu, D. Cheng, T. S. Williams, J. Severino, I. M. De Rosa, L. Carlson and R. F. Hicks, *Carbon*, 2013, **57**, 11–21.
33 J. Lee, D. Lim, W. Choi and S. Dimitrijev, *J. Nanosci. Nanotechnol.*, 2012, **12**, 1507–1512.
34 J. Y. Yook, J. Jun and S. Kwak, *Appl. Surf. Sci.*, 2010, **256**, 6941–6944.
35 V. K. Abdelkader, S. Scelfo, C. García-Gallarín, M. L. Godino-Salido, M. Domingo-García, F. J. López-Garzón and M. Pérez-Mendoza, *J. Phys. Chem. C*, 2013, **117**, 16677–16685.
36 G. Kalita, S. Adhikari, H. R. Aryal, D. C. Ghimre, R. Afre, T. Soga, M. Sharon and M. Umeno, *Phys. E*, 2008, **41**, 299–303.
37 C. H. Tseng, C. C. Wang and C. Y. Chen, *Chem. Mater.*, 2007, **19**, 308–315.
38 W. J. Zhang, X. Y. Li, X. Wang, D. G. Yu, W. H. Qian, Y. T. Ye and Z. Y. Wang, *Appl. Mech. Mater.*, 2012, **217–219**, 272–275.
39 A. O. Lobo, S. C. Ramos, E. F. Antunes, F. R. Marciano, V. J. Trava-Airoldi and E. J. Corat, *Mater. Lett.*, 2012, **70**, 89–93.
40 H. Wei, Y. Wei, Y. Wu, L. Liu, S. Fan and K. Jiang, *Nano Res.*, 2013, **6**, 208–215.
41 N. T. Alvarez, P. Miller, M. Haase, N. Kienzle, L. Zhang, M. J. Schulz and V. Shanov, *Carbon*, 2015, **86**, 350–357.
42 A. P. Inc, *API-60, Materials Safety Data Sheet*, Benicia, CA, 94510, 2012.
43 USPTO, US7008555, 2006.
44 J.-H. Pöhls, M. B. Johnson, M. A. White, R. Malik, B. Ruff, C. Jayasinghe, M. J. Schulz and V. Shanov, *Carbon*, 2012, **50**, 4175–4183.
45 ASTM D3039/D3039M-14, *Standard Test Method for Tensile Properties of Polymer Matrix Composite Materials*, ASTM International, West Conshohocken, PA, 2014, http://www.astm.org.
46 ASTM D638-14, *Standard Test Method for Tensile Properties of Plastics*, ASTM International, West Conshohocken, PA, 2014, http://www.astm.org.
47 P. D. Bradford, X. Wang, H. Zhao, J.-P. Maria, Q. Jia and Y. T. Zhu, *Compos. Sci. Technol.*, 2010, **70**, 1980–1985.
48 W. Liu, X. Zhang, G. Xu, P. D. Bradford, X. Wang, H. Zhao, Y. Zhang, Q. Jia, F.-G. Yuan, Q. Li, Y. Qiu and Y. Zhu, *Carbon*, 2011, **49**, 4786–4791.
49 Q. Jiang, X. Wang, Y. Zhu, D. Hui and Y. Qiu, *Composites, Part B*, 2014, **56**, 408–412.
50 Y. N. Liu, M. Li, Y. Gu, K. Wang, D. Hu, Q. Li and Z. Zhang, *Carbon*, 2013, **65**, 187–195.
51 X. Wang, P. D. Bradford, W. Liu, H. Zhao, Y. Inoue, J.-P. Maria, Q. Li, F.-G. Yuan and Y. Zhu, *Compos. Sci. Technol.*, 2011, **71**, 1677–1683.
52 X. Wang, Q. Jiang, W. Xu, W. Cai, Y. Inoue and Y. Zhu, *Carbon*, 2013, **53**, 145–152.
53 L. Zhang, X. Wang, R. Li, Q. Li, P. D. Bradford and Y. Zhu, *Compos. Sci. Technol.*, 2016, **123**, 92–98.
54 N. P. Zschoerper, V. Katzenmaier, U. Vohrer, M. Haupt, C. Oehr and T. Hirth, *Carbon*, 2009, **47**, 2174–2185.
55 L. Xu, Z. Fang, P. Song and M. Peng, *Appl. Surf. Sci.*, 2010, **256**, 6447–6453.
56 W. Liu, X. Zhang, G. Xu, P. D. Bradford, X. Wang, H. Zhao, Y. Zhang, Q. Jia, F.-G. G. Yuan, Q. Li, Y. Qiu and Y. Zhu, *Carbon*, 2011, **49**, 4786–4791.
57 Z. Zhang, K. Peng and Y. Chen, *eXPRESS Polym. Lett.*, 2011, **5**, 516–525.
58 P. C. Ma, J.-K. K. Kim and B. Z. Tang, *Compos. Sci. Technol.*, 2007, **67**, 2965–2972.
59 E. Ciecierska, A. Boczkowska, K. J. Kurzydlowski, I. D. Rosca and S. Van Hoa, *J. Therm. Anal. Calorim.*, 2013, **111**, 1019–1024.
60 L. Shechter and J. Wynstra, *Ind. Eng. Chem.*, 1956, **48**, 86–93.
61 P. Pötschke, N. P. Zschoerper, B. P. Moller and U. Vohrer, *Macromol. Rapid Commun.*, 2009, **30**, 1828–1833.
62 Q. Jiang, Y. Li, J. Xie, J. Sun, D. Hui and Y. Qiu, *Composites, Part B*, 2013, **45**, 1275–1281.
63 L. Zhang, X. Wang, W. Xu, Y. Zhang, Q. Li, P. D. Bradford and Y. Zhu, *Small*, 2015, 3830–3836.

64 W. Liu, H. Zhao, Y. Inoue, X. Wang, P. D. Bradford, H. Kim, Y. Qiu and Y. Zhu, *Composites, Part A*, 2012, **43**, 587–592.
65 Y.-N. N. Liu, M. Li, Y. Gu, K. Wang, D. Hu, Q. Li and Z. Zhang, *Carbon*, 2013, **65**, 187–195.
66 Q. Liu, M. Li, Y. Gu, Y. Zhang, S. Wang, Q. Li and Z. Zhang, *Nanoscale*, 2014, **6**, 4338–4344.
67 T. H. Nam, K. Goto, Y. Yamaguchi, E. V. A. Premalal, Y. Shimamura, Y. Inoue, S. Arikawa, S. Yoneyama and S. Ogihara, *Composites, Part B*, 2016, **85**, 15–23.
68 T. Q. Tran, Z. Fan, A. Mikhalchan, P. Liu and H. M. Duong, *ACS Appl. Mater. Interfaces*, 2016, **8**, 7948–7956.
69 P. Liu, Y. F. Tan, D. C. M. M. Hu, D. Jewell and H. M. Duong, *Mater. Des.*, 2016, **108**, 754–760.
70 J. Min, J. Y. Cai, M. Sridhar, C. D. Easton, T. R. Gengenbach, J. McDonnell, W. Humphries and S. Lucas, *Carbon*, 2013, **52**, 520–527.
71 R. Malik, Y. Song, N. Alvarez, B. Ruff, M. Haase, B. Suberu, A. Gilpin, M. Schulz and V. Shanov, in *Symposium UU – Plasma and Low-Energy Ion-Beam-Assisted Processing and Synthesis of Energy-Related Materials*, 2013, vol. 1574, p. mrss13-1574-uu03-04.
72 J. W. Kim, G. Sauti, E. J. Siochi, J. G. Smith, R. A. Wincheski, R. J. Cano, J. W. Connell and K. E. Wise, *ACS Appl. Mater. Interfaces*, 2014, **6**, 18832–18843.